phys. stat. sol. (b) **236**, No. 1, 151–165 (2003) / **DOI** 10.1002/pssb.200301416

F centers in LiF: A nuclear magnetic resonance study

T. Klempt, O. Kanert, and **D. Suter***

Universität Dortmund, Fachbereich Physik, 44221 Dortmund, Germany

Received 31 May 2002, revised 11 September 2002, accepted 16 September 2002
Published online 13 February 2003

PACS 61.82.Ms, 76.30.Mi, 76.60.Es

Ionizing radiation like γ-rays, electrons, or swift heavy ions create a variety of point defects in dielectric materials. The largest fraction of the defects consists of the paramagnetic F centers. Here, we study those F centers in LiF by nuclear magnetic resonance. Nuclear spin relaxation (T_1) measurements serve as a probe for the F centers offering the possibility to investigate their dynamics as a function of temperature and irradiation dose. Moreover, one is able to estimate the content of the paramagnetic defects from the T_1-data over a wide range of concentration. We further observed and analyzed radiation annealing occurring at temperatures above 360 K.

1 Introduction

Ionizing irradiation like high-energy electrons, ions, and photons, creates a large variety of different defects in dielectric materials. Among the primary defects, F centers, i.e. electrons at an empty anion site, are formed relatively easily. F centers in alkali halides have widely been studied over the last fifty years [1–16] by optical absorption spectroscopy, nuclear magnetic resonance (NMR), electron paramagnetic resonance (EPR), and other techniques. As these studies have shown, the F center EPR spectra show orientation dependent hyperfine splittings due to the interaction with the neighboring lithium and fluorine atoms. The optical spectra were investigated, and the density of the different kinds of crystal defects like F, F_2 or F_3 centers can be determined from the intensity of the respective absorption lines [4, 15, 17, 18]. Some dynamical studies and annealing experiments were performed [1, 19], which show that the F centers are stable at room temperature, but recombine at temperatures higher than 360 K [19]. NMR studies showed clear evidence that besides the F centers molecular fluorine and metallic lithium clusters were created [12].

The main focus of this work is an investigation of the formation of F centers in LiF, the coupling of the F center spins to lattice dynamics and to nuclear spins, the relaxation of nuclear spins by the F centers, and the annihiliation of F centers by thermal annealing. Most of these informations are obtained by measurements of the nuclear spin-lattice relaxation (NSR) time constant T_1 of the ^{7}Li and ^{19}F spins. The results were supplemented by optical absorption measurements.

We applied three types of ionizing radiation: high-energy photons, electrons, and heavy ions, which create different damage patterns. The γ-photons, which were taken from a ^{60}Co decay (energy E = 1.17 and 1.33 MeV, dose D = 1 kGy − 5 MGy) and the electrons (E = 20 MeV, D = 100 kGy)

* Corresponding author: e-mail: Dieter.Suter@physik.uni-dortmund.de, Tel.: +49 231 755 3512, Fax.: +49 231 755 3516

 0370-1972/03/23603-0151 $ 17.50+.50/0

create a homogeneous distribution of defects. In contrast irradiation with swift heavy ions like ^{208}Pb (E = 29 MeV/u) causes an inhomogeneous distribution [15, 20–22] consisting of a core region of 2–4 nm diameter around the ion track, where the high defect concentration leads to aggregates of defects and Li clusters, while the halo region with a diameter of 20–30 nm contains mostly F centers and their agglomerates [15, 23].

2 Relaxation through paramagnetic impurities

Nuclear spin relaxation in ionic crystals like lithium fluoride is often dominated by paramagnetic impurities. After averaging over the orientation dependence, the direct relaxation rate for nuclear spins at a distance r from a paramagnetic center is [24, 25]

$$\overline{P}(r) = Cr^{-6} \quad \text{with} \quad C = \frac{2}{5}\,\gamma_S^2\gamma_I^2\hbar^2 S(S+1)\,\frac{\tau_e}{1+\omega_L^2\tau_e^2}\,, \tag{1}$$

where ω_L is the Larmor frequency of the nuclear spin, S the spin of the paramagnetic center, $\gamma_S(\gamma_I)$ represents the gyromagnetic ratio of the electron (nuclear) spin, and τ_e denotes the correlation time of the electronic spin.

If the density of paramagnetic centers is small, the direct relaxation is very slow for the majority of the nuclear spins, since the rate decreases with the sixth power of the distance. In this case, the relaxation is dominated by spin diffusion which transports magnetization via flip flop processes from the quickly relaxing nuclear spins close to the paramagnetic centers to the more distant nuclear spins. The spin diffusion coefficient D_s can be calculated by Bloembergens [26] approximation,

$$D_s \approx \frac{a^2}{50T_2} \tag{2}$$

where a presents the closest distance between two identical spins and T_2 is the related nuclear spin spin relaxation time, which can determinied either experimentally by measuring the free induction decay (FID) or theoretically from the dipolar second moment [27]. We have to emphasize that the factor 50 in Eq. (2) is only an estimation for a cubic lattice and one type of spin species. Other authors like Lowe and Gade [28] found an other factor with a weak orientation dependence. The total evolution of the nuclear magnetization density $m_z(r,t)$ to the thermal equilibrium m_{z_0} can be described by [27, 29, 30]

$$\left(\frac{\partial m_z}{\partial t}\right) = D_s\nabla^2 m_z - C(m_z - m_{z_0})\,r^{-6}\,. \tag{3}$$

In the slow spin-diffusion case, the relaxation can be described approximately by a single spin lattice relaxation time T_1 for the nuclear spin system, which is given by [6, 24, 29]

$$\frac{1}{T_1} = \frac{8}{3}\,\pi N_p C^{1/4} D_s^{3/4} = \frac{8}{3}\,\pi N_p\left(\frac{2}{5}\,S(S+1)\,\gamma_S^2\gamma_I^2\hbar^2 D_s^3\,\frac{\tau_e}{1+\omega_L^2\tau_e^2}\right)^{1/4} = A\left(\frac{\tau_e}{1+\omega_L^2\tau_e^2}\right)^{1/4}, \tag{4}$$

where N_p is the density of paramagnetic centers.

If $\omega_L\tau_e > 1$, Eq. (4) can be written as

$$\frac{1}{T_1} = A\omega_L^{-1/2}\tau_e^{-1/4}\,, \tag{5}$$

while in the fast electronic relaxation range ($\omega_L\tau_e < 1$) Eq. (4) becomes

$$\frac{1}{T_1} = A\tau_e^{1/4}\,. \tag{6}$$

Finally, one should note that the spin diffusion approach is based on rather open parameters, i.e. principally a perfect agreement between the approach and the experimental data cannot be expected.

Table 1 F center concentration and NSR times of ^{19}F and ^{7}Li in γ -irradiated (^{60}Co, $E = 1.17$ MeV and 1.33 MeV) LiF single crystals. The calculated (according to Eq. (4)) and experimental NSR times T_1 were determined for a magnetic field of 1.22 T at a temperature of 4.2 K.

N_F [10^{17} cm^{-3}]	^{19}F-T_1 calc. [s]	^{19}F-T_1 exp. [s]	^{7}Li-T_1 calc. [s]	^{7}Li-T_1 exp. [s]
0.47 ± 0.01	1940 ± 250	381 ± 4	3400 ± 600	1282 ± 24
2.21 ± 0.05	480 ± 70	392 ± 18	850 ± 150	–
7.4 ± 0.2	87 ± 11	115 ± 2	150 ± 20	156 ± 3
9.1 ± 0.2	55 ± 10	66 ± 1	100 ± 20	–
17.3 ± 0.4	19 ± 3	17 ± 1	33 ± 5	25 ± 1

Neverteless, the validity of Eq. (4) for F centers in LiF was confirmed surprisingly good in a separate work, where the different parameters of Eq. (4) were determined independently [27, 31]. The main results of the work are listed in Table 1.

3 Experimental

Optical absorption measurements were carried out on a Cary 2300 spectrometer at room temperature. The NMR measurements were performed in different superconducting magnets with magnetic fields of 1.22 T, 4.08 T, 4.75 T, 8.46 T, and 14.09 T, and in a field cycling spectrometer covering a magnetic field ranging from 4×10^{-4} T to 0.7 T [32]. High field measurements below room temperature were performed in a continuous flow cryostat (Oxford Instruments), while for measurements above room temperature a home-built high temperature probe was used. The magic angle spinning (MAS) experiments were performed at 14.09 T in a Varian InfinityPlus system. The T_1 measurements were performed with an saturating recovery pulse sequence, where the nuclear spin magnetization M_z is distroyed by a train of rf-pulses. After a recovery time t, $M_z(t)$ is monitored by a $\pi/2$-pulse. We should emphasize, that the recovery of M_z was always observed to be exponential. EPR spectra were measured by means of a home-built EPR spectrometer working at 14 GHz. The irradiation of the crystals with heavy ions was performed with the UNILAC accelerator at the Gesellschaft für Schwerionenforschung (GSI) in Darmstadt (Germany) or with the GANIL accelerator in Caen (France). The samples under irradiation with γ-rays were prepared at the Institut für Oberflächenmodifizierung (IOM) in Leipzig (Germany), and electron irradiation was carried out with an electron accelerator at the University of Bonn (Germany). All beams hit the LiF target perpendicular to the (100) surface at room temperature. After irradiation the samples were stored at room temperature to obtain a thermal equilibrium of the generated defects.

4 Creation of defects

The concentration of F centers can be measured directly by optical absorption or indirectly through the nuclear spin lattice relaxation rate T_1^{-1}. While optical absorption allows a precise measurement of low defect concentrations through the specific absorption lines, NMR measurements are more precise at high concentrations. Then optical density is often oversized for absorption measurements. NMR measurements are also useful if the optical quality of the sample is not suitable for optical investigations. Figure 1 summarizes the NMR measurements of the dose dependence for irradiation with γ-rays from a ^{60}Co decay, i.e. with photon energies $h\nu$ = 1.17 MeV and 1.33 MeV. For each dose value, a single crystal, cutted from the same starting material, was irradiated with the respective dose. Spin lattice relaxation rates were then measured at room temperature for the two nuclear probes at three different magnetic field strengths: ^{7}Li at $B_0 = 8.46$ T, ^{19}F at $B_0 = 4.09$ T, and ^{19}F at $B_0 = 1.22$ T.

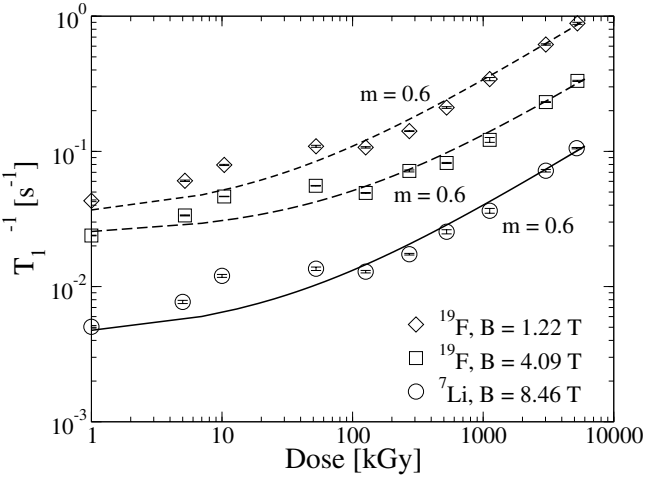

Fig. 1 Dose dependence of the NSR rate of ^{7}Li and ^{19}F. The LiF single crystal was irradiated with γ-rays from a ^{60}Co decay. The error bars are smaller than the points. The background relaxation rates T_{1bg}^{-1} are, 0.032 s^{-1}, 0.024 s^{-1} and 0.0042 s^{-1} for ^{19}F(1.22 T), ^{19}F(4.09 T) and ^{7}Li(8.46 T), respectively.

All three data sets show the same dependence on the dose. The data can be fitted with the relation $T_1^{-1} = T_{1bg}^{-1} + a_0(D/D_0)^{0.6}$, with D_0 = 1 kGy. T_{1bg}^{-1} represents the background relaxation of the crystal, which is due to paramagnetic impurities other than F centers, and $a_0 = 0.0049\,\mathrm{s}^{-1}$ (^{19}F, $B_0 = 1.22$ T); $0.0017\,\mathrm{s}^{-1}$ (^{19}F, $B_0 = 4.09$ T); $0.00057\,\mathrm{s}^{-1}$ (^{7}Li, $B_0 = 8.46$ T) is a proportionality constant that describes the relaxation efficiency of the F centers. The exponent (= 0.6) was found to be the same in all three cases. The sublinear increase of the F center density with the dose indicates that at higher densities the F centers agglomerate. As F_2 centers are not paramagnetic, they do not contribute to the NMR relaxation.

While the distribution of F centers caused by irradiation with electrons and γ-rays is homogeneous, heavy ions create an inhomogeneous defect distribution: the defects density is highest along the ion track and shows a non-monotonic variation with the penetration depth. The dependence of the defect density on the dose is also different, typically exhibiting a saturation behavior that can be described by a Poisson law [15, 20, 21]

$$N_F = N_F^{sat}(1 - \exp(-k\Phi)). \tag{7}$$

An alternative approach is given by the Lidiard relation [33]

$$N_F = N_F^{sat}\sqrt{1 - \exp(-k\Phi)}. \tag{8}$$

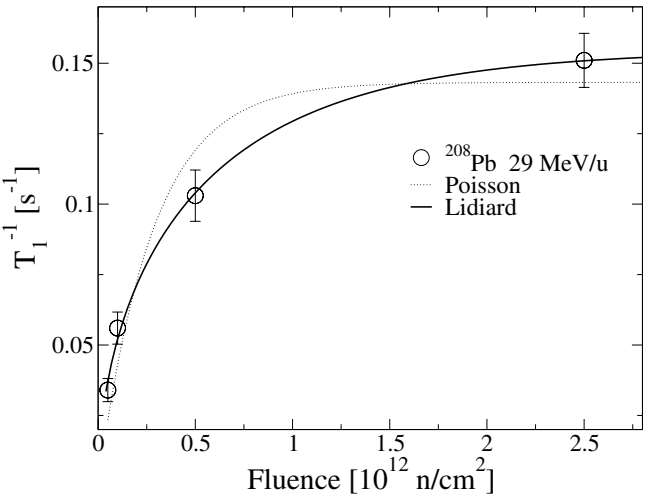

Fig. 2 Dose dependence of the NSR rate of ^{7}Li. The crystal was irradiated with ^{208}Pb ions with an energy of 29 MeV/u. The fluence was varied from 10^{10} n/cm^2 to 2.5×10^{12} n/cm^2. A fluence Φ of 10^{10} n/cm^2 of ^{208}Pb ions with an energy of 29 MeV/u corresponds to a dose of 146 kGy. The solid curve represents the Lidiard relation (Eq. (8)) while the dashed curve obeys the Poisson law (Eq. (7)).

In both cases, N_F^{sat} describes the maximum concentration of F centers and k the efficiency of the irradiation process. In difference to Lidiard, the Poisson relation assumes that each ion creates a cylindrical defect region, in which the F center concentration is saturated. If the fluence of the ions is large enough, the defect regions start to overlap. This leads to the Poisson relation (Eq. (7)), while Lidiards assumption of a homogeneous defect distribution leads to the relation (Eq. (8)).

We have performed nuclear spin relaxation (NSR) measurements on samples irradiated with ^{208}Pb ions with an energy of 29 MeV/u, corresponding to 6 GeV per ion. The results are summarized in Fig. 2. Supposing $1/T_1 \propto N_F$ according to Eq. (4), we compared the two theoretical curves, which favors the Lidiard relation (Eq. (8)) more than the Poisson law (Eq. (7)). The best agreement was obtained for $T_{1_{sat}}^{-1} = 0.155\ s^{-1}$ and $k = 1.2 \times 10^{-12}\ cm^2/n$. Using the same proportionality constant for the relaxation efficiency of the F centers as in the γ irradiated LiF crystal, we can extrapolate the F center density by knowing the spin lattice relaxation rate T_1^{-1}. This corresponds to a saturation density of $N_F^{sat} \approx 5.5 \times 10^{18}\ cm^{-3}$.

5 Motional processes

Nuclear spin relaxation is able to probe sensitively dynamical processes in the lattice. In this section we discuss nuclear spin relaxation data that probe the dynamics of the electronic F center spins, which are assumed to couple to the lattice predominantly by a two-phonon Raman process.

5.1 Background ions

The crystals used for these studies were manufactured by Korth Kristalle (Germany). The overall purity is specified as better than 99.9%. According to the manufacturer, the main impurities are Mg^{2+} ions, which are not paramagnetic. Moreover, the manufacturer stated that the samples contain some ppm manganese ions (Mn^{2+}) located preferentially at alkali ion sites [34]. Mn^{2+} has an electron configuration [Ar] $3d^5$ with a ground state $^6S_{5/2}$ [34, 35], i.e. Mn^{2+} is a paramagnetic center, and therefore contributes to the nuclear spin relaxation via fluctuating I–S interaction. Measured EPR spectra of our samples exhibit a corresponding weak signal with a g-value of 2 and a width of $\Delta B \approx 150$ G, in accord with observations of Mehendra et al. [36]. They have measured a simple ESR line of Mn^{2+} in LiF with a linewidth of about 200 G. One should note, however, that depending on the Mn^{2+} concentration the ESR line of Mn^{2+} exhibits a hyperfine structure [37] which was not observed in our experiments. As we did not detect further ESR signals we assume that Mn^{2+} are the main paramagnetic impurities in our samples.

To distinguish the Mn^{2+}-induced background contribution from that of the F centers, we first measured the relaxation of the nominally pure crystals. The crystals used for these studies were cutted to a size of 1.5 mm × 5 mm × 10 mm and subsequently annealed by heating to T_a = 1000 K for 60 minutes. The same treatment was used for the crystals irradiated with electrons.

Relaxation times were measured at two different magnetic fields (1.22 T and 4.08 T) as a function of temperature. Figure 3 summarizes the results for temperatures between 4 K and 300 K. The data show that the additional annealing process had a relatively small effect on the relaxation rate. The two series measured at different fields show a qualitatively similar behavior, exhibiting a strong temperature dependence: At low temperatures ($T < 20$ K), the relaxation rate increases as $T_1^{-1} \propto T^{2.4\pm0.1}$. It reaches a maximum at 18 K in a magnetic field of 1.22 T and at 23 K in a magnetic field of 4.08 T. At higher temperatures, the relaxation rate decreases as $T_1^{-1} \propto T^{-(0.29\pm0.03)}$. This temperature dependence is qualitatively similar to ^{19}F relaxation in NaF or SrF_2 due to Mn^{2+} [38, 39], and supports the idea that the background relaxation is primarily due to manganese ions.

The maximum of the nuclear spin relaxation rate occurs when the correlation time of the perturbation matches the nuclear Larmor frequency, i.e. $\omega_L \tau_e = 1$ according to Eq. (4). Using the maximum condition, we determined the correlation times τ_e of the Mn^{2+} spins to 3.3×10^{-9} s at 18 K and 9.7×10^{-10} s at 23 K, respectively.

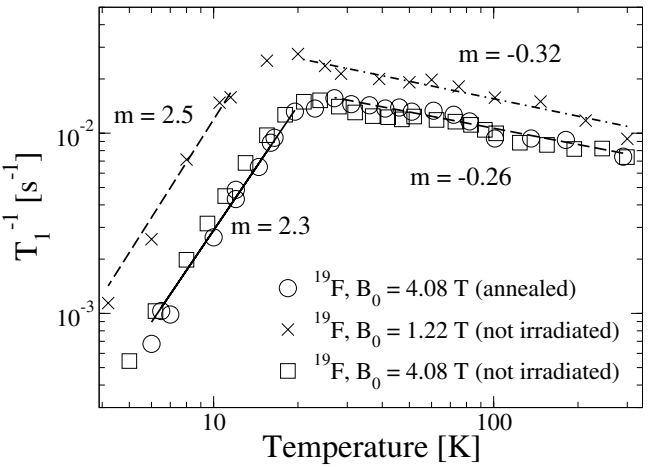

Fig. 3 Temperature dependence of the ^{19}F spin lattice relation rate T_1^{-1} of a pure LiF crystal. The sample was investigated before the crystal was irradiated with 20 MeV electrons and after the crystal was annealed at temperatures up to 1000 K. The measurements were performed at 1.22 T and 4.08 T, respectively.

As shown by Eq. (5), the nuclear spin relaxation rate depends on the electron spin correlation time τ_e as $T_1^{-1} \propto \tau_e^{-1/4}$ in the slow motion regime $\omega_L \tau_e \gg 1$. Therefore the low-temperature behavior of the relaxation rate is given by $\tau_e^{-1} \propto T^9$, as expected for a two-phonon Raman process at temperatures far below the Debye temperature θ_D [35, 38, 40].

For the fast motion regime, $\omega_L \tau_e \ll 1$, the nuclear spin relaxation rate should depend on τ_e as $T_1^{-1} \propto \tau_e^{1/4}$ according to Eq. (6). This points to a variation of the electronic correlation time as $\tau_e^{-1} \propto T^{(1.15 \pm 0.15)}$. The temperature dependence is significantly weaker than for a Raman process in the high temperature range, where $\tau_e^{-1} \propto T^2$ is predicted [35]. Similar properties were observed at atomic hydrogen in fused silica [41], and were explained by local vibrations of the paramagnetic impurities [42, 43].

On the low-temperature side, the data measured at the two different fields differ by a factor of 2.5; on the high-temperature side, the ratio is close to 1.3. The observation can be explained by the dependence of T_1^{-1} on the correlation time τ_e. At low temperatures, the ratio should be equal to the square root of the ratio of the Larmor frequencies $\left(\sqrt{\frac{\omega_L(4.08\,\mathrm{T})}{\omega_L(1.22\,\mathrm{T})}} = 1.8 \right)$ according to Eq. (5), while at higher temperatures, the ratio should be equal 1 (Eq. (6)). The fact, that this is not exactly true indicates, that correlation times of the manganese ions depend weakly on the magnetic field, as discussed in [35, 40].

Equation (4) can be used to estimate the concentration N_p of the paramagnetic centers. Using the condition $\omega_L \tau_e = 1$ Eq. (4) results in

$$N_p = \frac{3}{8\pi}\, T_1^{-1} \left(\frac{2}{5}\, S(S+1)\, \gamma_S^2 \gamma_I^2 \hbar^2 \right)^{-1/4} D_s^{-3/4} \left(\frac{\tau_e}{2} \right)^{-1/4}. \tag{9}$$

Using the measured T_1 and calculated τ_e values with T_1 = 36 s (18 K), 66 s (23 K) as given by Fig. 3 and $\tau_e = 3.3 \times 10^{-9}$ s, 9.7×10^{-10} s for the magnetic field of 1.22 T and 4.08 T respectively as obtained from the maximum condition, we maintain a manganese ion concentration of $N_p \approx 10^{16}$ cm^{-3} within the range specified by the crystal manufacturer.

5.2 F center dynamics

For the investigation of F center dynamics, we used LiF samples that were irradiated either with high energetic electrons (D = 100 kGy) or with γ-rays (D = 1 kGy − 5 MGy). Measurements of ^{19}F and ^{7}Li NSR times T_1 were performed in magnetic fields of 1.22 T and 4.08 T over the temperature range from 4–300 K.

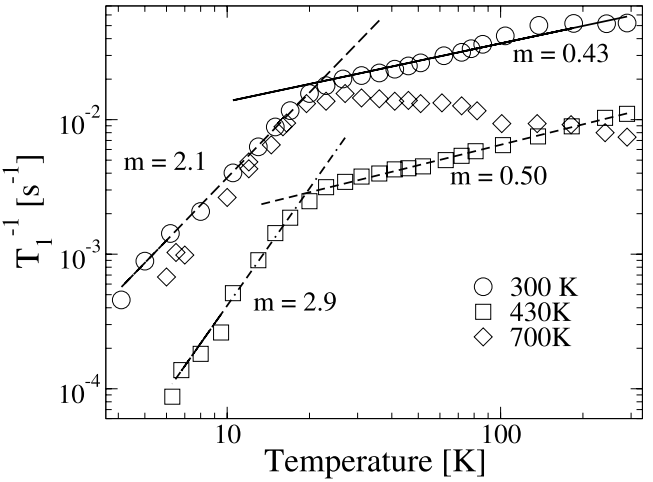

Fig. 4 Temperature dependence of the ^{19}F spin lattice relaxation rate T_1^{-1} in a magnetic field of 4.08 T. (○) sample e-irradiated (E = 20 MeV, D = 100 kGy); (□) same sample, annealed at 430 K for 20 min; (◇) same sample, after further annealing at 700 K for 20 min (complete annealing).

Figure 4 shows the observed relaxation rates for a sample irradiated by electrons with a dose of 100 kGy, measured in a magnetic field of 4.08 T. As discussed in section IV, at this dose, the contribution of the F centers to the NSR rate is remarkable larger than that of the background ions. After measuring the temperature dependence of the relaxation time T_1, the sample was heated at 430 K for 20 min to anneal part of the F centers, and cooled down again to repeat the NSR measurements. After the second series of measurements, the sample was treated at 700 K to anneal completely all the F centers, and the relaxation was measured again.

At temperatures below 20 K, the NSR rate of the irradiated sample increases as $T_1^{-1} \propto T^{2.1}$. As discussed for the background relaxation, this corresponds to an increase of $\tau_e^{-1} \propto T^{8.4}$, in reasonable agreement with the behavior expected for a Raman process [10]. At temperatures $T > 20$ K, the temperature dependence of T_1 becomes weaker ($T_1^{-1} \propto T^{0.43}$), which corresponds to a $\tau_e^{-1} \propto T^{1.7}$-law for the F center dynamics. The relaxation rates of the partially annealed sample exhibit a temperature dependence that is closely similar to that of the irradiated sample, while the magnitude of the relaxation is slower in the entire temperature range. This behavior can be explained with a reduction of the number of F centers.

The two data sets also show a slight difference in the temperature dependence: On the low-temperature side, the exponent increases from 2.1 to 2.9 corresponding to an increase of the exponent for the electronic correlation time from 8.4 to 11.6. On the high-temperature side, the exponent increases from 0.43 to 0.5, corresponding to 1.7 and 2.0 for τ_e. The weaker temperature dependence for the more concentrated sample may be due to interactions between the electronic spins, causing flip-flop processes [35] which are nearly independent of temperature. Hence, the total temperature dependence of τ_e consisting of the flip-flop part and a temperature dependent spin lattice part becomes weaker for rising concentrations of the F centers. This effect increases with decreasing temperature and increasing F center concentration. In consequence, at low temperature and high concentration, the electronic correlation time τ_e shows a weaker temperature dependence than expected from the contribution of the electronic spin-lattice relaxation alone.

Another effect that can contribute to the weaker temperature dependence at higher F center concentrations is their tendency to form weakly bound clusters [11, 44]. As discussed in detail by Warren et al. [11], large concentrated F centers tend to cluster involving fast cross-relaxation processes between the paramagnetic spins. In consequence, the resulting correlation time of the complex exhibits an unusual temperature and field dependence. In addition, a distribution of such clusters results in a corresponding broad distribution of electronic spin correlation times of the clusters leading to a modified temperature dependence of the effective τ_e [10, 11]. The temperature and field dependence of the nuclear spin relaxation rate induced by these F center clusters reflects this complex dynamics.

The ^{19}F NSR rate of the fully annealed sample shows the same temperature dependence as the unirradiated crystal (see Fig. 3). It is surprising that the relaxation rate is higher than that of the partially annealed sample at temperatures below 150 K. One normally assumes that different centers contribute additive rates to the nuclear spin relaxation, $T_1^{-1} = T_{1_{Mn}}^{-1} + T_{1_F}^{-1}$. Annealing (i.e. reducing N_F) should therefore lower the overall relaxation rate. The data in Fig. 4 clearly do not allow such a separation.

A possible interpretation could be that the F centers tend to couple antiferromagnetically with the Mn^{2+} ions, thus creating a diamagnetic complex and lowering the total relaxation rate. The manganese ions tend to cluster to negatively charged defects compensating their positive charge [34]. An alternative mechanism of the observed effect could be the formation of F_2 center complexes showing a diamagnetic ground state [45]. The formation of such centers will lead to the observed decrease of $1/T_1$. However, the explanation of the surprising effect is still an unsolved problem.

A similar behavior was observed for samples irradiated with γ-rays. Figure 5 shows the temperature dependence of the ^{19}F relaxation for dose rates between 1 kGy and 5 Mgy, measured in a field of 4.08 T. The NSR rate of the 1 kGy sample appears to be mainly determined by the contribution of the manganese ions. At dose rates >126 kGy, the F centers start to dominate the relaxation. The data clearly show that the temperature dependence becomes weaker as the F center concentration increases, again indicating the appearance of energy-conserving flip-flop processes between the electron spins and the additional relaxation on F center clusters.

Equation 4 allows us to calculate the electronic correlation time τ_e from the nuclear spin relaxation rate $1/T_1$:

$$\tau_e = \frac{2}{5}\, S(S+1)\, \gamma_S^2 \gamma_I^2 \hbar^2\, \frac{D_s^3}{\omega_L^2} \left(\frac{8}{3}\, \pi N_p T_1\right)^4 . \tag{10}$$

Using the F center concentration $N_p = 7.4 \times 10^{17}\mathrm{cm}^{-3}$ (126 KGy), $1.7 \times 10^{18}\mathrm{cm}^{-3}$ (1122 KGy), and $4.5 \times 10^{18}\ \mathrm{cm}^{-3}$ (5 MGy) determined from optical absorption measurements, we obtained a temperature dependence of τ_e which is summarized in Fig. 5. The temperature dependence of the 126 kGy irradiated sample calculated by Eq. (10) shows the same behavior than that of isolated F centers in KCl measured directly by means of pulsed ESR experiments [10]. The main features of the correlation times τ_e observed in the different samples are a power-law dependence at low temperatures, with an exponent that decreases from m = 5.7 to m = 3.9 as the dose increases from 0.1 to 5.0 MGy, in agreement with the behavior of the electron-irradiated samples. At temperatures above 60 K, the temperature dependence of the samples with higher doses becomes very weak and even negative. The difference between the different concentrations decreases at higher temperatures, indicating that the effect of correlations between the centers decreases.

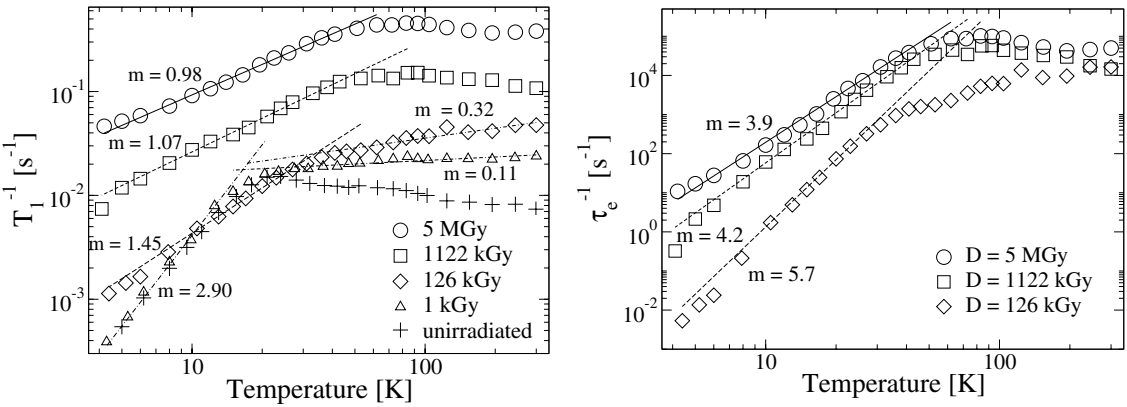

Fig. 5 Temperature dependence of the ^{19}F spin lattice relaxation rate T_1^{-1} (left) and of the correlation rates τ_e^{-1} (right) for a γ-irradiated sample in a magnetic field of 4.08 T. The dose rate was between 1 kGy and 5 MGy. The correlation time τ_e was calculated by Eq. (4).

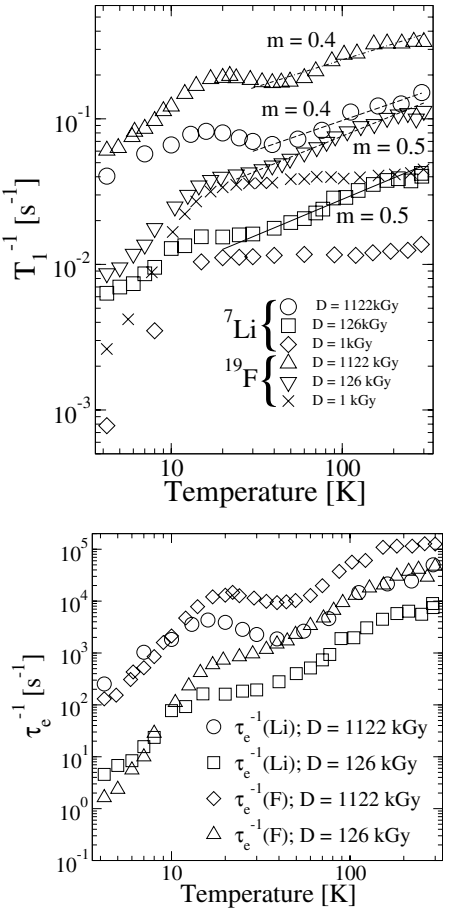

Fig. 6 Temperature dependence of the ^{19}F and ^{7}Li spin lattice relaxation rates T_1^{-1} (above) and of the correlation rates τ_e^{-1} (below) for a γ-irradiated sample in a magnetic field of 1.22 T. The dose rate was between 1 kGy and 1122 kGy. The correlation time τ_e was calculated according to Eq. (4).

The temperature dependence of the NSR rate for γ-irradiated samples with dose rates of 1 kGy, 126 kGy and 1122 kGy was also measured in a magnetic field of 1.22 T, for ^{19}F as well as for ^{7}Li nuclei. The results are summarized in Fig. 6, together with the corresponding electronic correlation times. The relaxation of ^{19}F is generally faster than that of ^{7}Li, as expected for the higher gyromagnetic ratio and faster spin diffusion. The temperature dependence, however, is quite similar. The remaining differences become particularly clear if one uses both data sets to calculate the electronic correlation time τ_e. At lower temperatures, they are identical within the experimental error. At temperatures above 20 K, they differ by almost an order of magnitude. Phonon contributions are known to become remarkable on $1/T_1$ at elevated temperatures ($T > 20$ K). As ^{19}F is a "dipolar" nuclear probe ($I = 1/2$) and ^{7}Li is a "quadrupolar" nuclear probe ($I = 3/2$) the resulting phonon-spin interaction can be different for the two probes. This may be the reason for the deviations in Fig. 6 above 20 K. However, a final interpretation is still an open problem.

Comparing these data to those measured at 4.08 T, we find that the cross-over from the low-temperature region characterized by a strong temperature dependence to the region exhibiting weak temperature dependence shifts to lower temperatures with decreasing fields. For temperatures $T > 40$ K, the rates increase as $T_1^{-1} \propto T^{(0.4-0.5)}$ and $\tau_e^{-1} \propto T^{(1.6-2.0)}$ in agreement with a Raman process in the high temperature range [35]. Below 20 K, the temperature dependence again is stronger. Between 20 K and 40 K we see only a weak temperature dependence (Fig. 6) for the samples irradiated with 126 kGy. Surprisingly, the sample with the highest defect concentration shows a non-monotonic temperature dependence with a decrease in the temperature range from 20 K to near 40 K. Similar properties were found at a magnetic field of 4.08 T (Fig. 5) at temperatures above 60 K. As the non-monotonic temperature dependence appears only at the highest defect concentration we assume that the observation is related to clustering effects [11]. A consistent interpretation, however, is still an open question.

6 Spin dynamics

6.1 Frequency dependence

The temperature-dependent measurements presented in the preceding section probe the dynamics of the spin lattice interaction. In this section, we investigate the dynamics of the spin degrees of freedom that are independent of lattice vibrations.

The NSR can be understood as a probe for the spectral density of the hyperfine coupling to the electron spins at the Larmor frequency. The frequency dependence and (by Fourier transformation) the

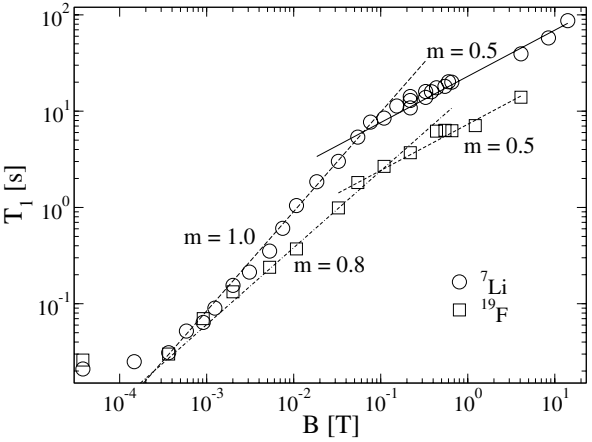

Fig. 7 Magnetic field dependence of the ^{19}F and ^{7}Li spin lattice relaxation times T_1 at room temperature. The sample was irradiated with γ-rays at a dose rate of 272 kGy. The measurements up to 0.65 T were performed in a field-cycling spectrometer, while above 0.65 T superconducting magnets were used.

time dependence of the electron spin correlation can therefore be probed by varying the magnetic field. Accordingly, we measured the relaxation times of ^{7}Li and ^{19}F at room temperature in a very wide range of magnetic fields between 4×10^{-5} T and 14.09 T. The sample was irradiated with γ-rays at a dose rate of 272 kGy. This corresponds to a F center concentration of $N_F = 9.1 \times 10^{17}$ cm^{-3}. The data, which are depicted in Fig. 7, show that the relaxation time T_1 is proportional to the square root of the magnetic field ($T_1 \propto \sqrt{B}$) between 0.04 T and 14.09 T. This is the field dependence predicted by Eq. (5) [24–26, 30] for a spin diffusion limited relaxation process, if the correlation time τ_e is field independent [6].

For magnetic fields lower than 0.04 T, the field dependence changes to $T_1(^{19}\mathrm{F}) \propto B^{0.8}$ and $T_1(^7\mathrm{Li}) \propto B$, respectively. A linear dependence of the NSR time on the Larmor frequency was predicted by Lowe [24] if the Larmor frequency (magnetic field) becomes smaller, and the fraction R/β approaches 1. R represents the averaged distance between the paramagnetic centers. $\beta = (C/D_s)^{1/4}$ [24] (see. Section 2) is a parameter for the relaxation process, which increases at lower magnetic fields. According to Lowe one has [24]

$$T_1^{-1} = 40.4 N_p^{4/3} C^{1/2} D_s^{1/2} \propto \omega_L^{-1} \propto B^{-1}\,, \tag{11}$$

where C is a constant (see Eq. (1)) and D_s is the spin diffusion coefficient as introduced in Section 2. For the ^{7}Li data, this relation provides an adequate description, although the numerical prefactor is closer to 300 than to 40 for our data. For ^{19}F, the dependence is clearly sublinear. At fields below 1 mT, the field dependence becomes weaker again, and both relaxation rates of ^{7}Li and ^{19}F level off and converge, indicating that the external field becomes comparable to the local fields, which are of the order of a few Gauss. The convergence of the spin lattice relaxation rates is caused by a cross relaxation process, occurring, if the resonance lines of the different nuclei start to overlap at small magnetic fields B_0 [46–48].

6.2 Quenching of the spin diffusion

In an earlier paper [27] we have shown experimentally that the nuclear spin relaxation in these systems is spin diffusion-limited obeying Eq. (4). In the following, we provide more direct evidence for spin diffusion effects by an experimental modification of D_s using the magic angle spinning (MAS) technique. The spin diffusion is part of the nuclear relaxation process, as can be seen from Eq. (3). Therefore, a quenching of D_s induces an increase of the NSR time T_1 (Eq. (4)). The sample rotation has a negligible effect on the direct relaxation, but if the rotation frequency exceeds the dipolar coupling strength (measured in frequency units), it averages the dipolar coupling to zero (in the limit of very high rotation rate) and thereby quenches the flip-flop processes, which are responsible for spin diffusion [49–52].

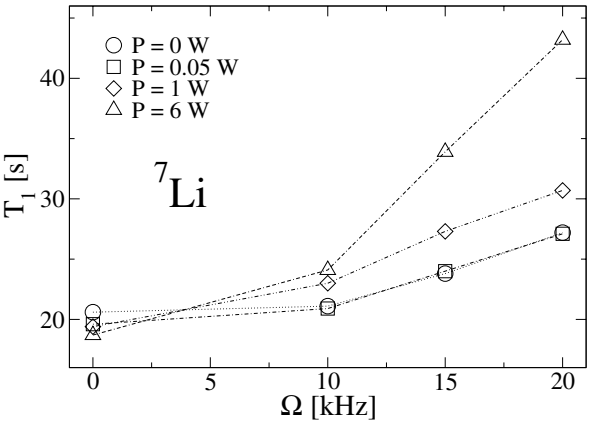

Fig. 8 Variation of the spin lattice relaxation times of ^{7}Li in a LiF crystal irradiated with a dose rate of 5 MGy γ-rays on the MAS rotation frequency Ω. The ^{19}F spins were partially decoupled during the relaxation period by rf irradiation P up to 6 W. Measurements were performed at room temperature in a magnetic field of 14.09 T.

We have measured the relaxation times of ^{7}Li and ^{19}F at room temperature in a sample irradiated with 5 MGy of γ-rays under magic angle spinning in a field of 14.09 T. For ^{7}Li, MAS reduced the measured linewidth from 19 kHz FWHH (static sample) to 0.9 kHz for the sample rotating at 20 kHz. As shown in Fig. 8, MAS rotation increases the relaxation time of ^{7}Li from 20 s for the static sample to 25 s at a sample rotation of Ω = 20 kHz. According to Eq. (4), the change in relaxation rate for the rotating sample is caused by a change of the spin diffusion. According to Eq. (4), the two variables depend on each other as

$$\frac{T_1(\Omega)}{T_1(0)} = \left[\frac{D_s(0)}{D_s(\Omega)}\right]^{3/4} . \tag{12}$$

This implies that the spin diffusion is suppressed by a factor of 1.35. Apparently the rotation speed of 20 kHz is not sufficient to quench the ^{7}Li spin diffusion, although the largest ^{7}Li–^{7}Li dipolar interaction, which can be calculated for the nearest-neighbor distance of 2.85 Å, is less than 11 kHz. This incomplete quenching of the ^{7}Li spin diffusion can be explained by taking into account that the homonuclear ^{7}Li–^{7}Li and ^{19}F–^{19}F couplings do not commute with the heteronuclear coupling between the ^{7}Li and ^{19}F spins [53]. A complete quenching of any of these interactions is only possible if the rotation rate Ω is large compared to all the interactions. From the crystal structure of LiF, we calculate the largest ^{7}Li–^{19}F coupling as 19 kHz and the ^{19}F–^{19}F interaction as 28 kHz. The maximum rotation rate (Ω = 20 kHz) is therefore large compared to the ^{7}Li–^{7}Li coupling (11 kHz), but does not exceed the ^{19}F–^{19}F interaction and is roughly equal to the heteronuclear coupling. This situation can be modified by rf-irradiation of the ^{19}F spins at the ^{19}F Larmor frequency. The design of the probe head limits the available rf power on the ^{19}F channel (which must be switched on for several minutes)

Table 2 Calculated spin diffusion coefficients and measured ^{7}Li spin lattice relaxation times at 14.09 T and 293 K for different spinning rates Ω and RF power P. The LiF crystal was irradiated with a dose rate of 5 MGy γ-rays.

P	0 kHz		10 kHz		15 kHz		20 kHz	
[W]	D_s [10^{-12} cm^2 s^{-1}]	T_1 [s]	D_s [10^{-12} cm^2 s^{-1}]	T_1 [s]	D_s [10^{-12} cm^2 s^{-1}]	T_1 [s]	D_s [10^{-12} cm^2 s^{-1}]	T_1 [s]
0	0.70	20.0	0.65	21.1	0.55	23.8	0.47	27.2
0.05	0.72	19.6	0.66	20.9	0.55	24.0	0.47	27.1
1	0.73	19.4	0.58	23.0	0.46	27.3	0.40	30.7
6	0.76	18.7	0.54	24.1	0.35	33.9	0.25	43.2

to a maximum of 6 W. This corresponds to a rf amplitude of $B_1 = 2.5$ G on the sample. Using the equation $\nu_R = \gamma B_1/2\pi$, we obtain a Rabi frequency of $\nu_R = 10$ kHz, which is smaller than the static linewidth. As shown in Fig. 8, ^{19}F decoupling has no effect on the relaxation rate of the static sample. However, the combination of ^{19}F decoupling and sample rotation provides an additional increase of the relaxation time T_1, indicating that the two spin species are partly decoupled. Apparently this level of decoupling is sufficient for an effective quenching of the ^{7}Li–^{7}Li coupling. But it only works well, if the Rabi frequency is in the range of the dipolar linewidth, narrowed by rotation Ω on the magic angle Θ.

On the basis of Eq. 12 we have calculated the spin diffusion constant D_s as a function of spinning rates Ω and RF power P. As shown in Table 2, the combination of sample rotation and ^{19}F decoupling reduces the spin diffusion by a factor of up to 3 under these experimental conditions.

We also measured the dependence of the ^{19}F NSR time on the MAS rotation, but found no significant variation. Apparently the available rotation speed is not high enough to affect significantly the ^{19}F–^{19}F coupling, in agreement with our conclusions from the ^{7}Li relaxation data.

7 Annealing

F centers in LiF are stable at room temperature, but at temperatures above 360 K their mobility is high enough to recombine with the hole centers. The annealing process can be monitored by NMR [27, 31, 54, 55]. In our experiments the temperature of the crystal was increased to the annealing temperature T_a and kept for a annealing time $\Delta = 20$ min. Then, the sample was cooled down to room temperature, and the respective concentration of the F centers was measured by NSR and optical absorption. If the thermally activated annealing is of first order, the process can be described by the rate equation [54]

$$\frac{\partial N_F}{\partial t} = -N_F(t)\, A \exp\ (-E_A/k_B T)\,, \tag{13}$$

where E_A describes the activation energy of the respective annealing process and A denotes the attempt frequency. Each annealing step reduces the F center concentration by a factor $\exp\,(-A \exp\,(-E_A/k_B T_a)\,\Delta)$. In our experiments we increased systematically the annealing temperature T_a, and the final density from the last step was the start value of the F-center concentration for the next step.

The NSR measurements of the F center density were performed at room temperature to avoid temperature-induced variations of T_1. If different types of paramagnetic centers contribute to the total NSR rate, we can write the relaxation rate after the i-th annealing step as

$$T_{1,i}^{-1} = \sum_{j=1}^{k} T_{1_{j,i-1}}^{-1} \exp\left[-A_j \exp\,(-E_{A_j}/k_B T_{ai})\,\Delta\right], \tag{14}$$

where the index j runs over the k distinguishable centers.

A first series of measurements was performed on a sample irradiated with electrons of an energy of 20 MeV and a dose rate of 100 kGy. During the stepwise annealing process, we measured the ^{19}F and ^{7}Li relaxation rate as well as the optical absorption. The results, which are summarized in Fig. 9 and Table 3, can be fitted with a single rate process with an activation energy $E_A = 0.60 \pm 0.07$ eV. These results indicate that the motion of the F centers is correlated with the diffusion of the Li-ions in the crystal, which has an activation energy of $E_A = 0.65$ eV [56, 57]. Optical absorption shows, that the annealing process is not completed at temperatures below 540 K. However, the optical data could not be evaluated at temperatures below 430 K, because the transmitted intensity was too small. Figure 9 shows, that the F center concentration, measured via optical absorption measurements, decreases up to a temperature of 540 K, while the NSR rate levels off at temperatures above 440 K indicating that the NSR relaxation is dominated by a fixed number of impurity ions.

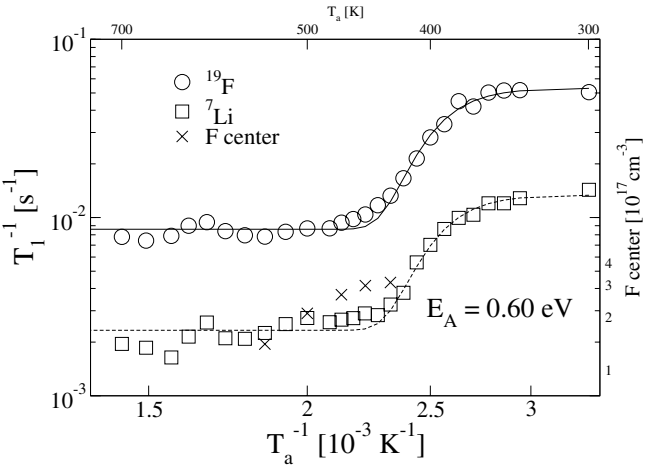

Fig. 9 Variation of T_1^{-1} of ^{7}Li (□) and ^{19}F (○) by stepwise annealing of a LiF sample irradiated with electrons (E = 20 MeV, D = 100 kGy). The NMR data are fitted by Eq. (14) using the parameter $E_A = 0.60 \pm 0.007$ eV. The F center concentration (×), which is indicated on the right ordinate, was measured by optical absorption.

A second series of measurements was performed on a sample irradiated with electrons of an energy of 0.5 MeV and a dose rate of 10 MGy. The NMR data in Fig. 10 exhibit two distinct annealing processes with activation energies of E_{A_1} = 1.0 eV and E_{A_2} = 1.5 eV. The other parameters are listed in Table 3. Both activation energies are higher than the activation energy of 0.6 eV observed for the low-dose irradiated sample, but variations of related activation energies up to 1.5 eV are frequently proposed [19, 58]. The third sample was irradiated with swift heavy ions (^{208}Pb, E = 29 MeV/u, $\Phi = 2.5 \cdot 10^{12}$ cm^{-2} [36.5 MGy]) The relaxation measurements were performed with ^{7}Li in a magnetic field of 4.75 T. The resulting data, presented in Fig. 10 and Table 3, show three distinct annealing steps with activation energies of 1.0, 1.5, and 1.7 eV. The first two energies match those from the sample irradiated with 0.5 MeV electrons. While the lowest activation energy could be interpreted again as a F center diffusion process, the other processes are not yet clear. A possible explanation of these processes could be an annealing of F center clusters. In summary, the respective annealing mechanism depends on the irradiation dose as well as on the kind of irradiation. Moreover, other parameters like temperature and the grown-in defects of the sample are also important for the annealing process.

Table 3 Fit parameters of the annealing experiments. The parameters for the different centers are calculated according to Eq. (14). $T_{1_{0,0}}^{-1}$ is the background rate. a1) and a2) represent the sample irradiated with electrons of a dose of 100 kG ($E = 20$ MeV) for ^{19}F and ^{7}Li, respectively. b) presents the 10 MGy (electrons, $E = 0.5$ MeV) sample and c) the sample irradiated with ^{208}Pb ions ($E = 29$ MeV/u, $\Phi = 2.5 \times 10^{12}$ cm^{-2}).

	j	A_j [min^{-1}]	$T_{1_{j,0}}^{-1}$ [s^{-1}]	E_{A_j} [eV]
a1)	0	–	$(8.6 \pm 0.4) \times 10^{-3}$	–
	1	$(6.6 \pm 0.5) \times 10^5$	$(4.6 \pm 0.1) \times 10^{-2}$	0.60 ± 0.07
a2)	0	–	$(2.3 \pm 0.2) \times 10^{-3}$	–
	1	$(7.4 \pm 0.5) \times 10^5$	$(1.1 \pm 0.1) \times 10^{-2}$	0.60 ± 0.07
b)	0	–	$(5.0 \pm 0.5) \times 10^{-4}$	–
	1	$(2.0 \pm 0.5) \times 10^6$	$(1.2 \pm 0.1) \times 10^{-1}$	1.0 ± 0.1
	2	$(5.0 \pm 0.5) \times 10^8$	$(1.0 \pm 0.1) \times 10^{-2}$	1.5 ± 0.1
c)	0	–	$(5.5 \pm 0.1) \times 10^{-4}$	–
	1	$(5.0 \pm 0.5) \times 10^6$	$(1.0 \pm 0.1) \times 10^{-1}$	1.0 ± 0.1
	2	$(5.0 \pm 0.5) \times 10^9$	$(2.0 \pm 0.1) \times 10^{-2}$	1.5 ± 0.1
	3	$(7.0 \pm 1.0) \times 10^9$	$(1.4 \pm 0.1) \times 10^{-3}$	1.7 ± 0.1

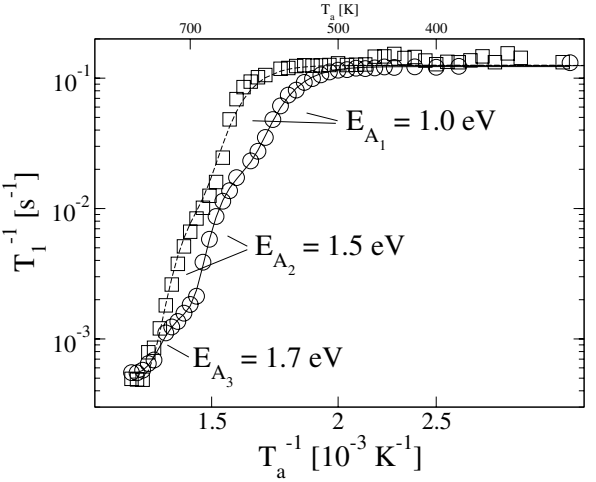

Fig. 10 Variation of the T_1^{-1} of ^{7}Li by stepwise annealing of an (□) electron irradiated sample ($E = 0.5$ MeV, D = 10 MGy) and a LiF sample irradiated with (○) ^{208}Pb ions with $E = 29$ MeV/u and a fluence $\Phi = 2.5 \times 10^{12}$ cm^{-2} corresponding to dose rate of $D = 36.5$ MGy. The NMR data are fitted by Eq. (14) using the fit parameter listed in Table 3.

8 Conclusions

We have investigated the formation of F centers in LiF by different types of ionizing radiation, the coupling among the electronic spins and nuclear spins, the coupling of the electronic spins to motional processes, diffusion of spin polarization depending on the nuclear decoupling, and the annealing of the F centers by a heat treatment. The experimental technique used in the present investigation was the nuclear spin lattice relaxation, which depends on the fluctuations of the electronic spins as well as on the spin diffusion within the nuclear spin system. Optical absorption measurements and nuclear spin relaxation data were used to determine the defect density in the samples as a function of the dose for different types of ionizing radiation, as well as their variation under thermal annealing. Variation of the irradiation procedure revealed a number of distinct recovery processes with corresponding distinct activation energies, which appear to be associated with different types of motional processes. Moreover, the effect of the spin diffusion on NSR could was observed by partial quenching of the spin diffusion process using rapid sample rotation at the magic angle and simultaneous nuclear spin decoupling by rf irradiation.

Acknowledgements We thank Prof. J. M. Spaeth and Prof. S. Schweizer for helpful discussion of F center dynamics, Prof. K. Schwartz for providing the ion-irradiated and the γ-irradiated samples, Prof. F. Fujara, Dr. A. Privalov and O. Lips for access to the field-cycling-spectrometer, Prof. H. J. Weber and H. P. Kreipe for experimental assistance with the optical absorption measurements. The work was supported financially by the Deutsche Forschungsgemeinschaft through the Graduiertenkolleg "Festkörperspektroskopie".

References

[1] C. J. Delbecq and P. Pringsheim, J. Chem. Phys. **21**, 794 (1953).
[2] A. F. Kip, C. Kittel, R. A. Levy, and A. M. Portis, Phys. Rev. **91**, 1066 (1953).
[3] A. M. Portis, Phys. Rev. **53**, 1071 (1953).
[4] R. T. Bate and C. V. Heer, J. Phys. Chem Solids **7**, 14 (1958).
[5] G. A. Noble, Phys. Rev. **118**, 1028 (1960).
[6] W. E. Blumberg, Phys. Rev. **119**, 1842 (1960).
[7] D. T. Teamey, W. E. Blumberg, and A. M. Portis, Phys. Rev. **119**, 1851 (1960).
[8] W. C. Holton and H. Blum, Phys. Rev. **125**, 89 (1962).
[9] R. Kaplan and P. J. Bray, Phys. Rev. **129**, 1919 (1963).
[10] D. W. Feldman, R. W. Warren, and J. G. Castle, Phys. Rev. **135**, A470 (1964).
[11] R. W. Warren, D. W. Feldman, and J. G. Castle, Phys. Rev. **136**, A1347 (1964).
[12] C. D. Knutson, H. O. Hooper, and P. J. Bray, J. Phys. Chem. Solids **27**, 147 (1966).

[13] N. G. Politov and L. F. Vorozheikina, Sov. Phys. – Solid State **12**, 277 (1970).
[14] L. H. Abu-Hassan and P. D. Townsend, Radiat. Eff. **98**, 479 (1986).
[15] K. Schwartz, C. Trautmann, T. Steckenreiter, O. Geiss, and M. Krämer, Phys. Rev. B **58**, 11232 (1998).
[16] G. Mallia, R. Orlando, C. Roetti, P. Ugliengo, and R. Dovesi, Phys. Rev. B **63**, 235102 (2001).
[17] C. J. Rauch and C. V. Heer, Phys. Rev. **105**, 914 (1957).
[18] P. Durand, Y. Farge, and M. Lambert, J. Phys. Chem. Solids **30**, 1353 (1969).
[19] N. Bouchaala, E. A. Kotomin, V. N. Kuzovkov, and M. Reichling, Solid State Commun. **108**, 629 (1998).
[20] A. Perez, E. Balanzat, and J. Dural, Phys. Rev. B **41**, 3943 (1990).
[21] C. Trautmann, M. Toulemonde, K. Schwartz, J. M. Constantini, and A. Müller, Nucl. Instrum. Methods B **164**, 365 (2000).
[22] E. A. Kotomin, V. N. Kuzovkov, and A. I. Popov, Radiat. Eff. Defects Solids **155**, 113 (2001).
[23] C. Trautmann, K. Schwartz, M. Constantini, T. Steckenreiter, and M. Toulemonde, Nucl. Instrum. Methods B **146**, 367 (1998).
[24] I. J. Lowe and D. Tse, Phys. Rev. **166**, 279 (1968).
[25] A. Abragam, Principles of Nuclear Magnetism (Oxford University Press, New York, 1961).
[26] N. Bloembergen, Physica **15**, 386 (1949).
[27] T. Klempt, S. Schweizer, K. Schwartz, O. Kanert, D. Suter, U. Rogulis, and J. M. Spaeth, Solid State Commun. **119**, 453 (2001).
[28] I. J. Lowe and S. Gade, Phys. Rev. **156**, 817 (1967).
[29] L. J. Humphries and S. M. Day, Phys. Rev. B **12**, 2601 (1975).
[30] W. E. Blumberg, Phys. Rev. **119**, 79 (1960).
[31] T. Klempt, S. Schweizer, K. Schwartz, O. Kanert, D. Suter, U. Rogulis, and J. M. Spaeth, Radiat. Eff. Defects Solids **155**, 159 (2001).
[32] O. Lips, A. F. Privalov, S. V. Dvinskikh, and F. Fujara, J. Magn. Reson. **148**, 22 (2001).
[33] A. B. Lidiard, Z. Phys. Chem. **206**, 219 (1998).
[34] G. D. Watkins, Phys. Rev. **113**, 79 (1959).
[35] A. Abragam and B. Bleaney, Electron Paramagnetic Resonance of Transition Ions (Clarendon Press, Oxford, 1970).
[36] P. C. Mehendru, G. D. Sootha, and V. Mitra, Radiat. Eff. **4**, 179 (1970).
[37] W. Low, Phys. Rev. **105**, 793 (1956).
[38] G. A. Persyn and A. W. Nolle, Phys. Rev. **140**, A 1610 (1965).
[39] J. B. Horak and A. W. Nolle, Phys. Rev. **153**, 372 (1967).
[40] K. J. Standley and R. A. Vaughan, Electron Spin Relaxation Phenomena in Solids (Plenum Press, New York, 1979).
[41] D. W. Feldman, J. G. Castle Jr., and G. R. Wagner, Phys. Rev. **145**, 237 (1966).
[42] J. Murphy, Phys. Rev. **147**, 241 (1966).
[43] L. Kevan and R. N. Schwartz, Time Domain Electron Spin Resonance (John Wiley & Sons, New York, 1979).
[44] R. E. Smallman and B. T. M. Willis, Philos. Mag. **2**, 1018 (1957).
[45] H. J. Paus and K. M. Strohm, J. Phys. C **13**, 57 (1980).
[46] R. V. Pound, Phys. Rev. **81**, 156 (1951).
[47] A. Abragam and W. G. Proctor, Phys. Rev. **109**, 1441 (1958).
[48] N. Bloembergen, S. Shapiro, P. S. Pershan, and J. O. Artman, Phys. Rev. **114**, 445 (1959).
[49] E. R. Andrew and R. A. Newing, Proc. Phys. Soc. **72**, 959 (1958).
[50] C. P. Slichter, Principles of Magnetic Resonance (Springer-Verlag, New York, 1961).
[51] H. Kessemeier and R. E. Norberg, Phys. Rev. **155**, 321 (1967).
[52] S. Hayashi, Solid State Nucl. Mag. Res. **3**, 323 (1994).
[53] D. Suter and R. R. Ernst, Phys. Rev. B **32**, 5608 (1985).
[54] F. Bell and R. Sizman, phys. stat. sol. **15**, 369 (1966).
[55] A. C. Damask and G. J. Dienes, Point Defects in Metals (Gordon & Breach, New York, 1963).
[56] Y. Haven, Rec. Trav. Chim. **69**, 1471 (1950).
[57] T. G. Stoebe and R. A. Huggins, J. Mater. Sci. **1**, 117 (1966).
[58] E. A. Kotomin, V. Kashcheyevs, V. N. Kuzovkov, K. Schwartz, and C. Trautmann, Phys. Rev. B **64**, 144108 (2001).